Supporting Information

Surface *versus* volume effects in luminescent ceria nanocrystals synthesized by oil in water microemulsion method

Carmen Tiseanu [*a], Vasile I. Parvulescu [*b], Magali Boutonnet [c], Bogdan Cojocaru [b] Philipp A. Primus [d], Cristian Teodorescu [e] , Conchita Solans [f] and Margarita Sanchez Dominguez [g]

[*a] National Institute for Laser, Plasma and Radiation Physics, P.O.Box MG-36, RO 76900, Bucharest-Magurele, Romania; [*b] University of Bucharest, Department of Chemical Technology and Catalysis 4 – 12 Regina Elisabeta Bvd., Bucharest 030016, Romania; [c]Kungliga Tekniska Högskolan (KTH), School of Chemistry, Div. of Chemical Technology, Teknikringen 42, SE-10044, Stockholm, Sweden; [d] Institute of Chemistry, Physical Chemistry, University of Potsdam, Karl-Liebknecht-Str. 24-25, 14476 Potsdam-Golm, Germany; [e] National Institute of Materials Physics, P.O. Box MG-7, 77125 Magurele, Romania; [f] Consejo Superior de Investigaciones Científicas (CSIC/IQAC), CIBER en Biotecnología, Biomateriales y Nanomedicina (CIBER-BBN), Jordi Girona 18-26, 08034 Barcelona, Spain; [g] Centro de Investigación en Materiales Avanzados, S. C. (CIMAV), Unidad Monterrey, Alianza Norte 202, 66600 Apodaca, Nuevo León, México.

[*] To whom correspondence should be addressed: tiseanuc@yahoo.com; v_parvulescu@yahoo.com.

.

Experimental details

Characterization. Particle size and morphology were investigated by High Resolution Transmission Electron Microscopy (HRTEM). The sample was prepared as follows: 0.5 mg of ceria powder were suspended in isopropanol (2 ml) and sonicated. For analysis a drop of this dispersion was deposited onto a holey formvar/carbon copper grid. Observation was carried out using a Field Emission Transmission Elentron Microscope, JEM-2200FS, 200 kV, with 0.19 nm resolution in TEM mode and 0.1 nm resolution in STEM mode and spheric abberration correction in STEM mode. Surface area and pore analysis were carried out at liquid nitrogen temperature with a Micromeritics ASAP 2020 Surface area and Porosity Analyzer. Before analysis the samples were outgassed at 150 ^{o}C for 12 h. Powder X-ray diffraction (XRD) patterns were recorded on a Schimadzu XRD-7000 diffractometer using Cu Kα radiation (λ = 1.5418 Å, 40 kV, 40 mA) at a scanning speed of 0.10 degrees min^{-1} in the 6 – 60 degrees 2Θ range inside an in-situ cell accessory. In situ calcination of the samples was carried out using the same apparatus in the 50 – 1000°C temperature range. DR-UV-Vis spectra were recorded at room temperature on a Analytik Jena Specord 250 spectrophotometer with an integrating sphere for reflectance measurements and Spectralon as the reflectance standard. DR-UV-Vis spectra of the catalysts were recorded in reflectance units and were transformed in Kubelka–Munk remission function F(R). Fourier transform infrared (FTIR) spectra were measured with a Thermo Electron Nicolet 4700 FTIR spectrometer with a Smart Accessory for diffuse reflectance measurements. The IR spectra were scanned in the region of 4000–400 cm^{-1} at the resolution of 4 cm^{-1}. The final spectra are an accumulation of 200 scans. Raman analysis was carried out with a Horiba Jobin Yvon - Labram HR UV-Visible-NIR Raman Microscope Spectrometer, with a DL 785-100 laser at 633, 514 and 488 nm and a catalytic cell for sample heating. In-situ measurements were carried out in the range 50 – 550 ^{o}C by heating the samples with a rate of 10°C/min and keeping a plateau of 10 minutes for collecting the spectra. X-ray photoelectron spectra (XPS) was measured in a Specs setup operating at a base pressure of low 10^{-10} mbar. Samples are constituted from powders dispersed onto carbon tapes. A flood gun operating at 1 eV energy and 0.1 mA electron current was used to ensure sample neutralization. XPS spectra were recorded by using unmonochromatized Mg K radiation (h = 1253.6 eV) and a Phoibos hemispherical energy analyzer of 150 mm radius operating at 30 eV pass energy for individual electron distribution curves (EDCs). Within these conditions, previous calibrations have shown an overall full width at half maximum (FWHM) of Ag 3d$_{5/2}$ lines of 1.37 eV.

Photoluminescence measurements. The photoluminescence (PL) measurements were carried out using a Fluoromax 4 spectrofluorometer (Horiba) operated in both the fluorescence and the phosphorescence mode. The repetition rate of the xenon flash lamp was 25 Hz, the integration window varied between 300 ms and 3 s, the delay after flash varied between 0.03 and 10 ms, and up to 100 flashes were accumulated per data point. The slits were varied from 0.001 nm to 10 nm in excitation as well as emission. PL decays were measured by using the "decay by delay" feature of the phosphorescence mode. Time resolved emission spectra (TRES) were recorded at room temperature using a wavelength tunable Nd:YAG-laser/OPO system (Spectra Physics/GWU) operated at 20 Hz as excitation light source and an intensified CCD camera (Andor Technology) coupled to a spectrograph (MS257

Model 77700A, Oriel Instruments) as detection system. The TRES were collected using the box car technique. The initial gate delay, (delay after laser pulse, δt) was set to 500 ns and the gate width δt was adjusted to 50 µs. The PL was detected in the spectral range of 500 nm < λ_{em} < 750 nm with a spectral resolution of 0.08 nm. Time resolved emission spectra (TRES) were also recorded using a nitrogen laser (emission wavelength at 337 nm, frequency of 20 Hz, model VSL-337ND-S from Spectra-Physics) an intensified CCD camera (Andor Technology) coupled to a spectrograph (Shamrock 303i , Andor Technology). Laser excited photoluminescence measurements were also performed at liquid nitrogen temperature (80 K). For the low-temperature measurements, the solid state samples were mounted on a cold finger attached to a liquid nitrogen Dewar.
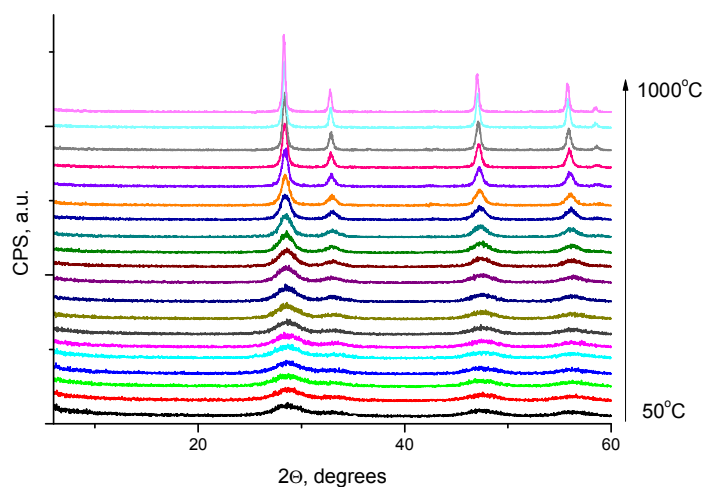
The PL decays were analyzed by fitting with a multiexponential function f(t) using the commercial software (OriginPro 8): $f(t) = \sum A_i \, exp(-t/\tau_i) + B$, where A_i is the decay amplitude, B is a constant (the baseline offset) and τ_i is the time constant of the decay i.
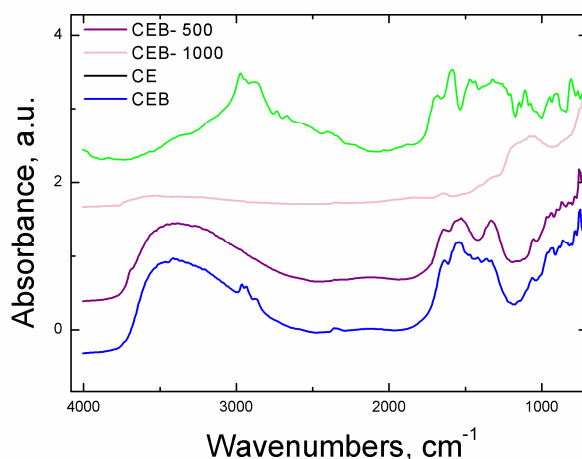
TGA
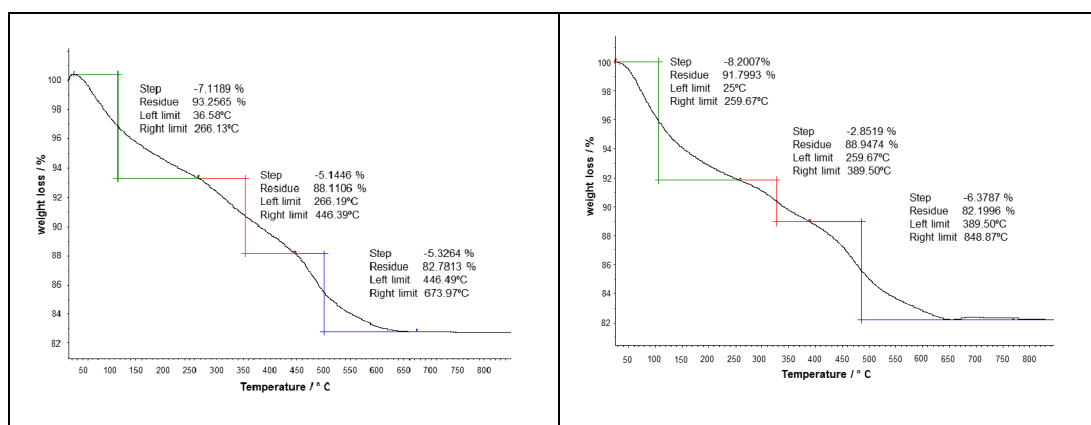
Fig. S1 (a). TGA of as-obtained, undoped ceria (CE) nanocrystals b) TGA of as-obtained, Eu- doped ceria (CEB) nanocrystals.

XRD

Fig. S2. In-situ XRD patterns with temperature of Eu-impregnated CeO_2 nanocrystals.

FTIR

Fig. S3. DRIFT spectra of CE, CEB, CEB- 500 and CEB- 1000 nanocrystals. Also included is the spectrum of Eu^{3+}- 2-ethylhexanoate.

FTIR analysis was carried to monitor the elimination of residual oil and organic phases from the microemulsion-derived precursor. FT-IR spectrum of europium ethyl hexanoate, exhibits strong absorption bands in the 1300-1600 cm^{-1} region due to symmetric and asymmetric stretching vibrations of the COO–groups (Figure S3). The bands within this spectral range seen in the spectra of doped (impregnated ceria) are therefore assigned mainly to the precursor. Following calcination, the relative intensity of these bands decrease ascertaining for the removal of organics. The presence of organics in the calcined sample may help in limiting the growth of the particle size.[1] The bands at 2800- 3000 cm^{-1} are assigned to CH stretching vibrations of the precursor which are completely removed at 500 °C. However they are still detectable with the impregnated samples calcined at 500 and 1000 °C that may also account for the small differences in the particle size of those compared with impregnated ceria (not shown). The relatively broad band centered at ~3000 cm^{-1} assigned to the –OH stretching vibration is relatively strong in all spectra except for CEB- 1000 (CEI-1000) where its intensity is drastically reduced.

1. J. Chandradass, B. Nam and K. H. Kim, *Colloid. Surface. A Physicochem. Eng. Aspect.* 2009, **348**, 130.
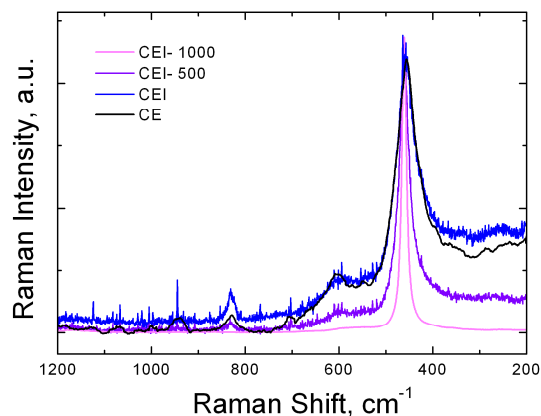
RAMAN

Fig. S4. Comparative Raman spectra of Eu-impregnated CeO_2 and CeO_2 nanocrystals. (λ_{ex}= 514 nm).
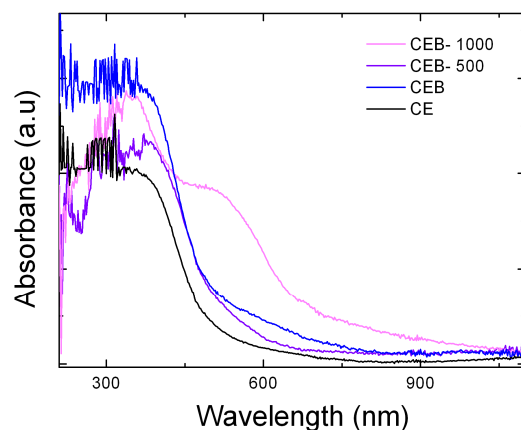
Absorption

Fig. S5. Absorption spectra of pure and europium doped CeO_2 nanocrystals.

UV/Vis absorption spectra. Cerium dioxide has high refractive index of 2.35, a band gap of 3. 2eV and absorbs strongly in the UV region (absorption threshold near 400 nm). From the diffuse reflectance reflectance spectra, a number of three bands at ~ 260, 280-290 and 320- 360 nm are observed with all ceria nanocrystals with absorption tails extending to the visible spectral range (Figures S2). Wuilloud et al.[1] suggested that the absorption of ceria originates from a charge transfer from O^{2-} to Ce^{4+}, that is, the O $2p^6$ - Ce $4f^0$ electronic transition (*vide infra*). The bands 320- 360 nm are assigned to charge transfer from bulk O^{2-} to Ce^{4+} transitions while the bands at ~260 nm may contain low coordination Ce^{3+} - oxygen and Ce^{4+} -oxygen charge transfer bands due to surface cerium oxygen species [2-5] Spectra were slightly shifted to the red following doping or calcination at 500 °C or to the blue spectra region with

concomitant appearance of a marked shoulder at about 520 nm at 1000 °C, while the intensity of 260

nm band was greatly reduced with calcination. No Eu^{3+} f-f absorption transitions could be evidenced.

1. E. Wuilloud, B. Delley and W.-D. Schneider, Y. Baer, *Phys. Rev. Lett.* 1984, **53**, 202.

2. A. Bensalem, F. Bozon-Verduraz, M. Delamar and G. Bugli, *Appl. Catal. A* 1995, **121**, 81.

3. B. M. Reddy and A. Khan, *Catal. Surv. Asia* 2005, **9,** 155.

4. F. Goubin, X. Rocquefelte, M. H. Whangbo, Y. Montardi, R. Brec, S. Jobic, *Chem. Mater.* 2004**, 16,** 662.

5. C. Binet, A. Bardi and J. C. Lavalley, *J. Phys. Chem.* 1994, **98**, 6392.

XPS spectra, assignement and deconvolution procedure. The initial paper by Burroughs et

al.[1] proposed both shake-down (lines labeled u, v) and parent states (lines labeled u''', v''') for the Ce 3d

spectrum in CeO_2, whereas states u', v' and u'', v'' were connected to collective excitations involving

Ce^{4+} 5d, 6s and 6p electrons. A subsequent work following Ce metal oxidation by XPS [2] proposed that

the parent peaks are v'' and u'', with u, u', v, v' corresponding to shake-down satellites involving charge

transfer from O 2p to Ce 4f or 5d; therefore, v''' and u''' would correspond to shake-up satellites. But this

assignment, not very firmly stated in the above reference, was not retained by most subsequent work [3-5]

where most authors agree that v''' and u''' represent the parent peaks, whereas v'', u'' and v, u represent

shake-down satellites corresponding to charge transfer of one O 2p electron on a Ce 4f orbital,

respectively to two O 2p electrons from the valence band onto two localized Ce 4f orbitals. There are

two objections that may be formulated to the above assignment: (i) an usually large chemical shift

between Ce^{3+} and Ce^{4+} parent lines, of some 12.3 eV results whereas the usual chemical shifts is of a

few eV usually [2]. (ii) the doublet (v, u), which is the most intense, if attributed to a $4f^2$ configuration,

would correspond to a multiple excitation involving *three* electrons: the photoelectron and the two

valence (or O 2p) electrons transferred on $4f^2$ states. These considerations pushed us to revisit the

attribution of the Ce 3d photoelectron peaks, with the help of the Ce^{3+} spectrum [3] and with the follow-up

of the Ce reduction by X-ray irradiation and hydrogen. [6-8]

The spectra from Figure 5a were deconvoluted by using six spin-orbit split Voigt doublets [9] with the

same spin-orbit splitting, lorentzian and gaussian widths. The complete formula for fitting is given in

Ref. 10. The branching ratio of the 3d lines was initially fixed to its theoretical value of 1.5, then

allowed to vary. The final value did not deviate too much from the theoretical value. The spin-orbit

splitting is 18.65 ± 0.04 eV. (Any attempt to perform such a deconvolution with only four components

failed with the constraints specified above; eventually, one may obtain a reasonable deconvolution by allowing quite different widths, unphysical values of branching ratios or strong deviations of the spin-orbit splitting from one doublet to another). The line widths obtained from deconvolution are about 2.7-2.9 eV, almost the double obtained in the same experimental conditions on a sputtered Ag foil (the explanation may be connected to the rough surface of the sample). The obtained line positions and amplitudes, together with their attributions, are listed in Table S1. In summary, with the labeling of Figure 5a, the Ce^{4+} parent doublets are (v", u"); the Ce^{4+} shake-down states are (v, u), the Ce^{4+} shake-up states are (v'", u'"). For Ce^{3+} the parent lines are (v', u'), the shake-down lines are (p, q) and the shake-up lines are (s, r). The shake-down satellites are shifted towards lower binding energy by about 6.2 eV for Ce^{4+}, and by about 5.25 eV for Ce^{3+}. The shake-up satellites are shifted towards higher binding energy by about 9.4 eV for Ce^{4+} and by 9.2 eV for Ce^{3+}. The line positions are not very different from one sample to another, although the energy was entirely allowed to vary. (The only exception was the energy of the shake-up satellite for Ce^{3+} in the calcinated sample, where the very low amplitude obtained from the fit obliged us to fix the energy value.). Finally, the chemical shift between parent lines of Ce^{3+} and Ce^{4+} results as 3.13 eV for CE, 3.20 eV for CEB and 3.40 eV for CEB- 1000. Binding energies and integral amplitudes extracted by deconvolution of the spectra from Figure 5a, together with the assignment proposed for each component are tabulated in Table S1.

Table S1. Binding energies and integral amplitudes extracted by deconvolution of the spectra from Fig. 10a, together with the assignment proposed for each component. $\varepsilon(p,f)$ represents the escaped photoelectron of p or f symmetry (according to dipole selection rules), V the valence band constituted mostly from O 2p orbitals and C the conduction band. Typical errors to be considered are below 0.01 eV for the binding energies and of about 2.5 % for the integral amplitudes.

Component	Parameter	CE	CEB	CEB-1000
Ce(4+) shake-down $3d_{5/2}{}^{-1}\varepsilon(p,f)V^{-1}4f^1C^0$	Binding Energy $3d_{5/2}$ (eV)	882.22	882.21	882.28
	Amplitude (cps x eV)	42 912	46 528	48 766
Ce(4+) $\varepsilon(p,f)V4f^0C^0$	Binding Energy $3d_{5/2}$ (eV)	888.39	888.46	888.63
	Amplitude (cps x eV)	13 078	15 215	17 458
Ce(4+) shake-up $3d_{5/2}{}^{-1}\varepsilon(p,f)V^{-1}4f^0C^1$	Binding Energy $3d_{5/2}$ (eV)	897.78	897.73	897.87
	Amplitude (cps x eV)	25 031	28 061	39 634
Ce(3+) shake-down $3d_{5/2}{}^{-1}\varepsilon(p,f)V^{-1}4f^2C^0$	Binding Energy $3d_{5/2}$ (eV)	880.01	880.06	879.93
	Amplitude (cps x eV)	20 050	21 802	15 697
Ce(3+) parent $3d_{5/2}{}^{-1}\varepsilon(p,f)V4f^1C^0$	Binding Energy $3d_{5/2}$ (eV)	885.26	885.26	885.24
	Amplitude (cps x eV)	31 747	36 800	25 594
Ce(3+) shake-up $3d_{5/2}{}^{-1}\varepsilon(p,f)V^{-1}4f^1C^1$	Binding Energy $3d_{5/2}$ (eV)	894.45	893.65	893.65
	Amplitude (cps x eV)	1 444	2 660	0

1 P. Burrougs, A. Hamnett, A. F. Orchard and G. Thornton, *J. Chem. Soc. Dalton Trans.* 1976, **17**, 1686.

2. G. Praline, B. E. Koel, R. L. Hance, H. I. Lee and J. M. White, *J. Electron Spectrosc. Relat. Phenom.* 1980, **21,** 17.

3.K. S. Sim, L. Hilaire, F. Le Normand, R. Touroude, V. Paul-Boncour, A. Percheron-Guegan, *J. Chem. Soc. Faraday Trans.* 1991, **8**7, 1453.

4. F. Le Normand, L. Hilaire, K. Kili, G. Krill, G. Maire, *J. Phys. Chem.* 1991, **92**, 2561.

5.A. Laachir, V. Perrichon, A. Badri, J. Lamotte, E. Catherine, J. C. Lavalley, J. El Fallah, L. Hilaire, F. Le Normand, E. Quémeré, G. N. Sauvion, O. Touret, *J. Chem. Soc. Faraday Trans.* 1991, **87**, 1601.

6. E. Paparazzo, *Surf. Sci. Lett.* 1990, **234**, L235.

7. E. Paparazzo, *Chem. Mater.* 2010, **22**, 4514.

8. F. Zhang, P. Wang, J. Koberstein, S. Khalid and S.-W. Chan, *Surf. Sci.* 2004, **563**, 74.

9. C. M. Teodorescu, J. M. Esteva, R. C. Karnatak, A. El Afif, A. *Nucl. Instrum. Meth. Phys. Res. A* 1994, **345.**

10. D. Mardare, D. Luca, C.M. Teodorescu and D. Macovei Surf. Sci. 2007, **601**, *4515*.

Emission spectra
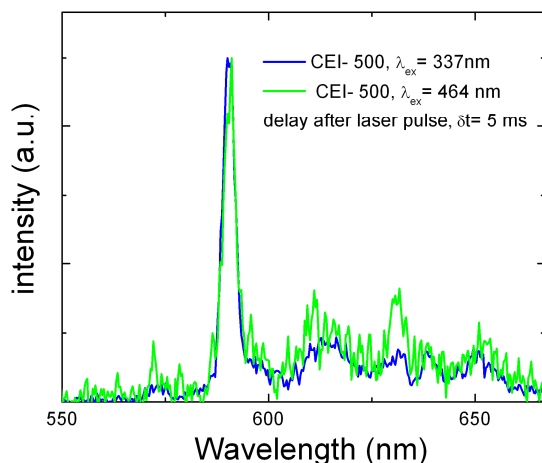
Fig. S6. Comparison between the delayed TRES spectra of CEB- 500 nanocrystals excited at 337 and 464 nm.

Analysis of the PL decays. To discard the $^5D_1$ emission related interference, we have first estimated the average PL lifetime of $^5D_1$ measured at λ_{em} =525- 540 nm at around 90- 100 µs. A value of ~ 1. 8 ms was determined from single exponential fitting of the tail of PL decay (λ_{ex}= 337, λ_{em}= 590 nm) which was assigned to the PL lifetime of HS europium species. The lifetime of the LS europium species was determined from the PL decays measured at λ_{em}= 579, 609, 630 nm with excitation at λ_{ex}= 464 nm. At λ_{em}= 579 nm, only the LS europium species contributes, whilst both LS and HS europium species emit in the spectral range of ~ 600-640 nm. A decay time of ca. 500- 525 µs was determined from the PL decay measured at λ_{em}=579 nm whilst two decay times, one at ca. 550 µs (with amplitude equal to ~ 90% from the total transient intensity) and other much longer at ca. 1.6- 1.8 ms (with amplitude equal to ~10% of the total transient intensity) were determined from the fitted transients at λ_{em}= 609 and 630 nm.
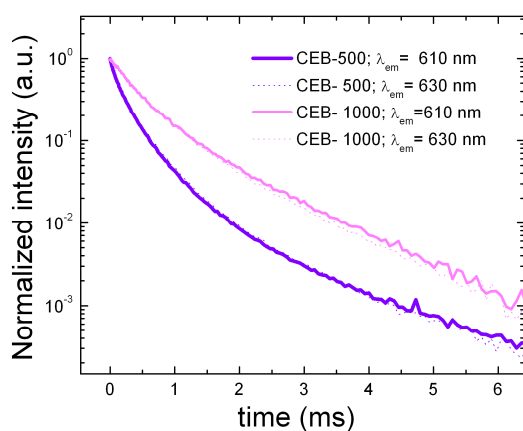
Fig. S7. Comparison between the PL decays of CEB- 500 and CEB- 1000 nanocrystals measured at 610 and 630 nm upon excitation at 464 nm.